

Clusters in the photodisintegration of ${}^9\text{Be}$

K. Shoda and T. Tanaka*

Laboratory of Nuclear Science, Tohoku University, Sendai 982-0826, Japan

(Received 1 December 1997)

The ground-state cross sections and angular distributions of ${}^9\text{Be}(\gamma,p)$, ${}^9\text{Be}(\gamma,t)$, ${}^9\text{Be}(\gamma,{}^3\text{He})$, and ${}^9\text{Be}(\gamma,d)$ are reported, together with the cross section for the ${}^9\text{Be}(\gamma,d)$ reaction to the first excited state. Qualitative discussions of these cross sections are made on the basis of a simple model which assumes free clusters in ${}^9\text{Be}$. This is similar to the two-cluster model used for ${}^6\text{Li}$ and ${}^7\text{Li}$ for which theoretical calculations have been made. Predictions on the basis of this model indicate the importance of clustering in the photodisintegration of ${}^9\text{Be}$, ${}^6\text{Li}$, and ${}^7\text{Li}$. The observed angular distributions are consistent with contributions due to $E1$ and $E2$ transitions. [S0556-2813(99)01801-4]

PACS number(s): 25.20.-x, 21.60.Gx, 27.20.+n

I. INTRODUCTION

The level structure of light nuclei can be described by the cluster model as well as by the single-particle shell model. These models can also be applied to describe the reaction mechanism involved in photonuclear reactions, and indeed many publications have applied the cluster model to ${}^6\text{Li}$ and ${}^7\text{Li}$. Studies of the momentum distribution of the alpha and deuteron clusters in the ground state of ${}^6\text{Li}$ using the ${}^6\text{Li}(e,e'd)$ reaction indicate that it can be modeled using an α - NN model [1]. Photodisintegration to ${}^3\text{He}+{}^3\text{H}$ and ${}^4\text{He}+{}^3\text{He}$ using linearly polarized photons [2] has been used to study cluster structure in ${}^6\text{Li}$ and ${}^7\text{Li}$. Measurements of the ${}^6\text{Li}(\gamma,d)$ and ${}^6\text{Li}(\gamma,t)$ reactions using tagged photons show evidence of both α - d and ${}^3\text{He}$ - t cluster components in ${}^6\text{Li}$ [3].

Theoretical analyses of these reactions have been made on the basis of a cluster model using potentials that have states forbidden by the Pauli principle [4,5]. This cluster nature of ${}^6\text{Li}$ has also been studied by inelastic ${}^3\text{He}$ scattering [6] and by quasifree α scattering [7]. An extensive analysis of the cluster nature in ${}^6\text{Li}$ has been made by Kukulin *et al.* [8].

The shell model nature of ${}^6\text{Li}$, ${}^7\text{Li}$, and ${}^9\text{Be}$ nuclei has been studied by means of the (γ,π^+) reaction. Highly excited spin-isospin flip states in ${}^6\text{Li}$, ${}^7\text{Li}$, and ${}^9\text{Be}$ have been studied by the (γ,π^+) reaction using about 200 MeV photons [9]. These states are analogs of residual states in ${}^6\text{He}$, ${}^7\text{He}$, and ${}^9\text{Li}$, respectively, left by π^+ emission. The (γ,π^+) reactions on these nuclei are well described by the impulse approximation. The results show that the group energy of the states in these nuclei can be explained by the shell model.

Photodisintegration of ${}^9\text{Be}$ leads to emission of many few-nucleon entities such as d , t , ${}^3\text{He}$, and α , in addition to single nucleons. This suggests the presence of clusters in ${}^9\text{Be}$ and the possible applicability of a cluster model. Since photon-induced reactions produce less distortion in the entrance channel than do nucleon-induced reactions, photonuclear studies might provide data that would more rigorously test the cluster model.

The ground state of ${}^9\text{Be}$ is considered to consist of a weakly bound unpaired $p_{3/2}$ neutron and a core of four $s_{1/2}$ and four $p_{3/2}$ nucleons. The photoabsorption cross section of ${}^9\text{Be}$ has been measured up to the photopion threshold [10]. In the region of the giant dipole resonance, the emitted particles are predominantly n , p , and α [11–14], with a non-negligible contribution by d , t , and ${}^3\text{He}$ [14–16].

Figure 1 shows the energy level diagram for the photoreactions of ${}^9\text{Be}$: the low-lying states in the residual nuclei are indicated. The reaction thresholds other than for (γ,n) and (γ,α) are greater than 16 MeV. Since the lowest $T_>$ state is at 14.393 MeV, excitations above this energy may involve population of both $T_<$ and $T_>$ isospin states.

The photoneutron cross section has been studied in three separate regions [11,13,17]: (1) threshold to 5 MeV, where sharp resonances correspond to direct excitations of the unpaired neutron; (2) 5–18 MeV, where coupling of the unpaired neutron to the ground state and the first excited state in ${}^8\text{Be}$ dominates; and (3) above 18 MeV, where a core neutron is emitted leaving ${}^8\text{Be}$ mainly in the 16.6 MeV excited state.

In all cases of photoneutron emission, subsequent α emission occurs due to the breakup of ${}^8\text{Be}$, which is described as a cluster of two α particles. In the region above 18 MeV, photoproton emission from the core is also possible: the similarity of the (γ,n) and (γ,p) reactions above 18 MeV supports the reaction mechanism mentioned above [13].

Photodeuteron and phototriton emission from ${}^9\text{Be}$ has been observed in the energy region above 20 MeV. For comparison with cluster model predictions for this nucleus, more precise experimental information on the photoemission of charged particles is needed.

In the present paper, good resolution cross sections and angular distributions have been measured for the photoemission of p , t , and ${}^3\text{He}$, leading to ground residual states, and of d , leading to the sum of the ground and first excited residual states. Since the reactions are measured specifically to the ground state [sum of the ground and first excited states for (γ,d)], the initial and final states are well defined. Thus there is a good basis for testing the cluster model for ${}^9\text{Be}$.

Since more than three clusters may contribute to the structure of ${}^9\text{Be}$, the theoretical analysis is not fully defined.

*Present address: Atomic Energy Research Institute, Nihon University, 7-24-1 Narashinodai, Funabashi 274-8501, Japan.

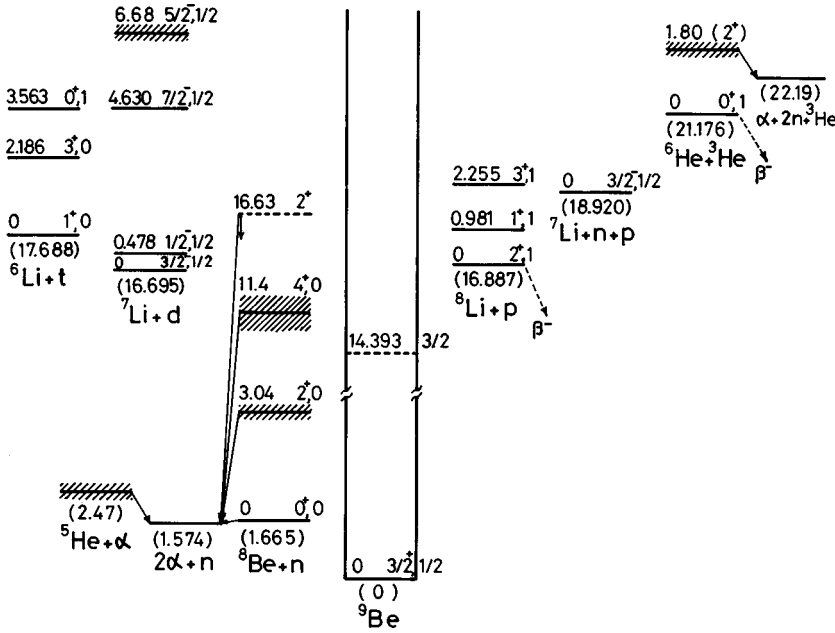


FIG. 1. Energy level diagram for the main photoreactions of ${}^9\text{Be}$. The energy is given in MeV. The threshold energies are shown in parentheses. The residual states in the lowest-energy region are also shown. Hatched states are resonance states. Unstable residual states are indicated by arrows showing breakup components. The ground state of ${}^6\text{He}$ and ${}^8\text{Li}$ is unstable for β^- decay with a half-life 806.7 ± 1.5 ms and 838 ± 6 ms, respectively. The lowest $T_{>}$ ($T = 3/2$) state is 14.393 MeV.

Thus, in the present work, a qualitative analysis with a simple cluster model is applied to ${}^9\text{Be}$. This method is then checked against ${}^6\text{Li}$ and ${}^7\text{Li}$, which have been well studied by the cluster model theory.

II. EXPERIMENTAL PROCEDURES

A 3.06-mg/cm²-thick ${}^9\text{Be}$ metal target was bombarded with electrons ranging from 21.0 to 39.0 MeV. Charged particles were momentum analyzed using a Browne-Buchner-type broad-range magnetic spectrometer and detected by a ladder of 100 Si(Li) solid state detectors set along the focal plane [18]. The relevant experimental parameters are shown in Table I. For those particles stopped in the detector, the energy loss was measured and, in combination with the momentum, particle identification was made using the relation

$$E = \frac{q^2}{2m} = \frac{Z^2(B\rho)^2}{m} \frac{e^2}{2c^2}. \quad (1)$$

Here E , q , m , and Z are the energy, momentum, mass, and charge number of the particle, B and ρ are the field strength and radius of the particle orbit in the magnet, and e and c are the elementary charge and the velocity of light.

TABLE I. Energy parameters of the experiments. E_e is kinetic energy of bombarding electron (resolution is 1.5%), and ΔE_e is energy step. θ is the detection angle.

Particle	p	d	t	${}^3\text{He}$
Energy distribution ($\theta = 125^\circ$)				
E_e (MeV)	21.5–28.0	21.0–35.0, 39.0	21.0–35.0	27.5–38.0
ΔE_e (MeV)	0.5	2.0	2.0	1.5
Angular distribution ^a				
E_e (MeV)	23.0	23.0	23.0	
		26.0	26.0	

^a $\theta = 42^\circ, 55^\circ, 67^\circ, 78^\circ, 90^\circ, 102^\circ, 113^\circ, 125^\circ, \text{ and } 138^\circ$.

Examples of spectra of the energy lost in the solid state detectors are shown in Fig. 2(a), which also shows particle identification. The lowest group does not correspond to the expected nuclear particles and is estimated to be ${}^4\text{He}^+$ ions. As shown by Eq. (1), the energies of protons and α particles are the same for the same B and ρ , so that they overlap in the spectra. A thin absorber of aluminized Mylar was inserted in front of the detector ladder in order to separate these two groups by virtue of the different energy loss in the absorber. Examples of such separation are shown in Fig. 2(b).

The energy distributions of p , d , t , and ${}^3\text{He}$, following electrodisintegration, were obtained from the yields of each particle group of the spectra from the 100 detectors on the ladder and spectrometer parameters. The proton spectra were thus obtained from data using the absorber to separate the α group as mentioned. The background in the spectrum from each detector was subtracted to determine the yield for each particle group.

Correction for the average energy loss by the particle passing through the target was made by adding the energy loss ($\Delta E_{1/2}$) corresponding to half the target thickness in the direction of emission. Examples of the results of the energy distribution of the emitted particles are shown in Figs. 3–6. In the figures, arrows show the end-point energy of particles leaving the residual nucleus in the ground, first, and second excited states.

III. RESULTS

Electronuclear reaction cross sections can be reduced to photonuclear reaction cross sections using a virtual photon spectrum [19]. The energy distributions of electroproduced particles are given by

$$I(E_x, E_e) = \sum_i \frac{d}{d\Omega} \sigma_{(\gamma, x_i)}(E_x, E_\gamma) N_{h\nu}(E_\gamma, E_e) \frac{dE_\gamma}{dE_{x_i}}, \quad (2)$$

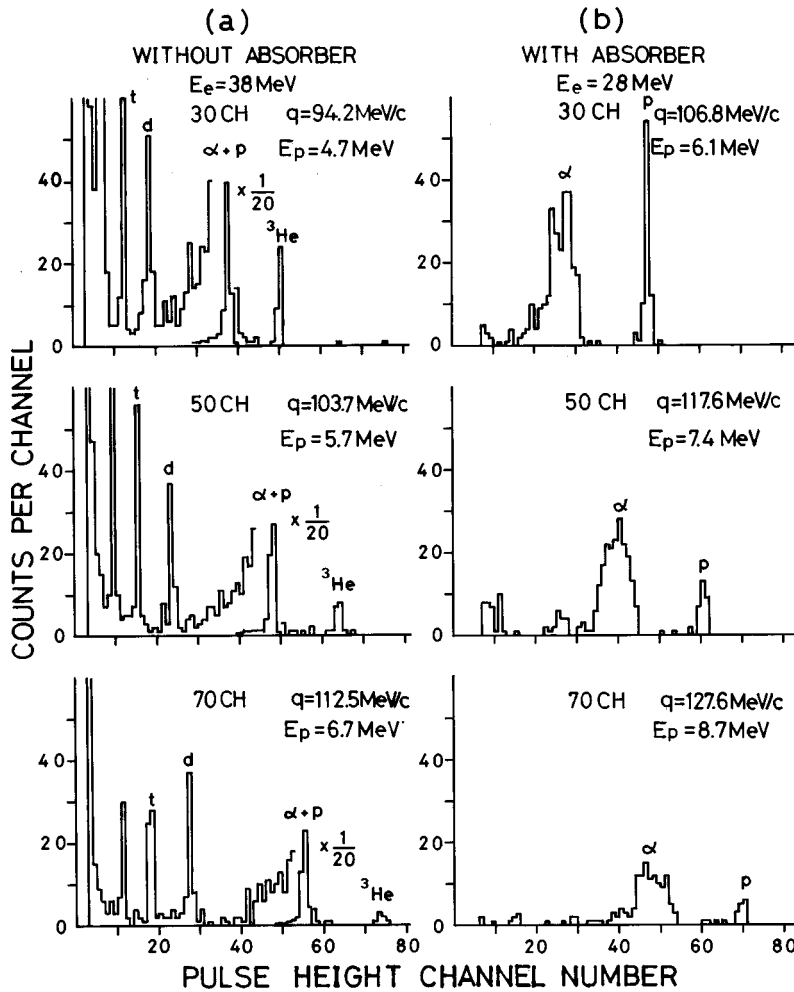


FIG. 2. Example of spectra of energy lost in solid state detectors. Data are shown at three positions, channels 30, 50, and 70 along the 100 detector ladder (proton momentum q is indicated for each channel). Identification of particle and incident energy of proton E_p are shown. (a) No absorber is set in front of the detector ladder. $E_e = 38 \text{ MeV}$. (b) Absorber is set in front of the detector ladder for separation between p and α . Here $E_e = 28 \text{ MeV}$.

where E_x is the kinetic energy of the emitted particle x with mass number a , E_γ is the photoexcitation energy, and $\sigma_{(\gamma, x_i)}(E_x, E_\gamma)$ is the cross section of the (γ, x_i) reaction at E_γ . The kinetic energy of the emitted particle x_i leading to the i th residual excited state with excitation energy of E_{R_i} is specified as $E_x = E_{x_i}$. Here $N_{h\nu}(E_\gamma, E_e)$ is the virtual photon spectrum associated with an electron of kinetic energy E_e [20]. The energy E_{x_i} is related to mass number A of the target nucleus, the threshold energy E_{th} , E_γ , and E_{R_i} as follows:

$$E_{x_i} = \frac{A-a}{A} \{E_\gamma - (E_{th} + E_{R_i})\}. \quad (3)$$

According to Eqs. (2) and (3), the end-point energy region ($E_x > E_{x_i}$) of the particle energy distribution $I(E_x, E_e)$ involves only particles leading to the residual ground state. Therefore the corresponding ground-state cross section $d\sigma_{(\gamma, x_0)}(E_\gamma)/d\Omega$ can be extracted from the end-point energy distribution using Eqs. (2) and (3). As seen in Fig. 1, the energies of the first excited states in the residual nuclei are large enough to apply the present analysis to obtain the ground-state cross sections for the (γ, p_0) , (γ, t_0) , and $(\gamma, ^3\text{He}_0)$ reactions.

For deuteron emission, the separation of the first excited and ground states is too small (0.4781 MeV) to permit separation. However, the second excited state is sufficiently well separated (4.630 MeV) to allow extraction of the sum of the ground and first excited states (γ, d_{0+1}) .

The energy of the particle is reduced by an amount that depends on the thickness experienced in the target. The resulting energy loss can be estimated by assuming a uniform production of particles in the irradiated target volume. This result suggests a significant modification in the energy distribution in the region within $\pm \Delta E_{1/2}$ of the end-point energy. However, the measured energy distributions have been corrected for the energy loss on the assumption that all the particles were emitted at a half thickness of the target. Thus, in order to avoid possible large errors in the analysis, the energy distribution in the region within $\pm \Delta E_{1/2}$ around the end-point energy was not used for the analysis of the cross sections. The energy $\Delta E_{1/2}$, which depends on the particle and its energy, is less than 0.1 MeV for p , 0.2 MeV for d , 0.4 MeV for t , and 1 MeV for ^3He in the present case.

A similar analysis was applied in order to obtain the angular distributions at the angles as shown in Table I. Here, the top 0.5 MeV of the energy distribution is not used, in order to minimize the effect of uncertainties in the particle energy spectrum and the virtual photon spectrum in the end-point energy region. The cross sections and angular distributions are shown in Figs. 7–13 together with previous data for

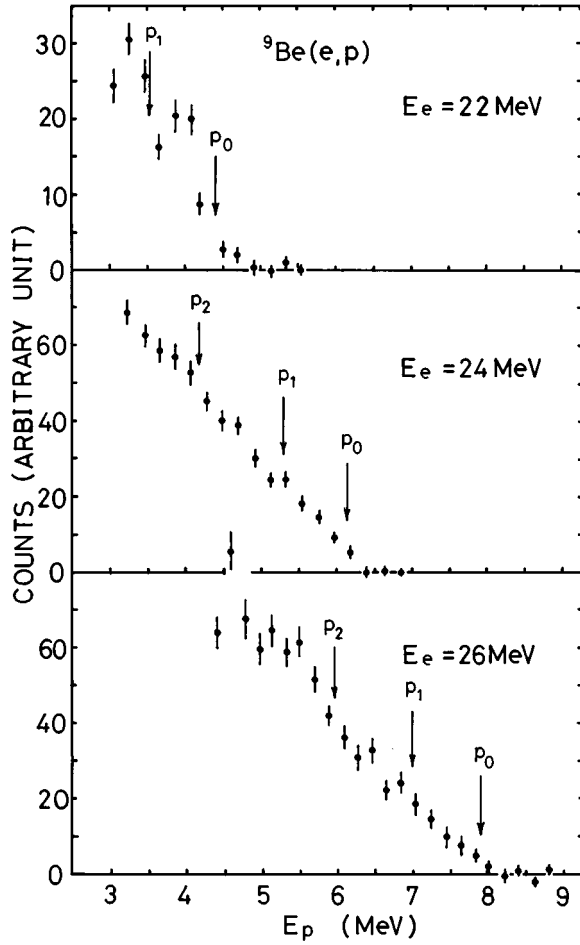


FIG. 3. Example of proton energy distributions by electron bombardment. The end-point energies of p_0 , p_1 , and p_2 are indicated by arrows.

comparison. The error bars in these figures are statistical only.

IV. DISCUSSION OF THE RESULTS

Photonuclear angular distributions may be expanded as

$$\frac{d\sigma}{d\Omega} = A_0 \sum_i a_i P_i(\cos \theta), \quad (4)$$

where $P_i(\cos \theta)$ are Legendre polynomials and a_i are coefficients determined by the interaction parameters. The connection between the terms in Eq. (4) and the photon multipoles and their interference terms are shown in Table II. Angular distribution coefficients a_i in Eq. (4) were determined by a χ^2 fit to the experimental results. The values $\chi^2 \equiv \sum_k \varepsilon_k^2 / \sigma_k^2$ are calculated by the deviation of the data points from the fitted curve (ε_k) and the standard deviation (σ_k) of the data points based on the statistics. The χ^2 are about 3 for the (γ, d_{0+1}) data shown in Fig. 12 and not sensitive to a selection of $i \leq 3$ and $i \leq 4$ for $P_i(\cos \theta)$. In the (γ, t_0) data shown in Fig. 13, χ^2 is about 1 for E_γ 21.5–22.5 MeV and about 8 for E_γ 24.0–25.5 MeV, and they are not sensitive to $i \leq 3$ and $i \leq 4$. In the (γ, p_0) data shown in Fig. 11, χ^2 is about 4 for both cases $i \leq 2$ and $i \leq 3$, but decreases to 0.2 for $i \leq 4$, indicating a better fitting. Thus, in the present

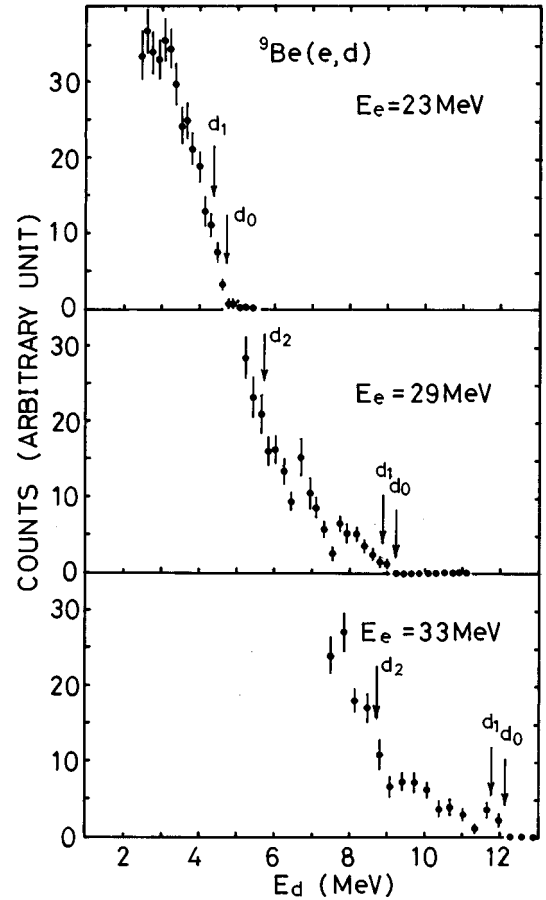


FIG. 4. Example of deuteron energy distributions by electron bombardment. The end-point energies of d_0 , d_1 , and d_2 are indicated by arrows.

results, the number of terms $P_i(\cos \theta)$ was limited to $i \leq 3$ for the ${}^9\text{Be}(\gamma, d_{0+1})$ and ${}^9\text{Be}(\gamma, t_0)$ data and to $i \leq 4$ for the ${}^9\text{Be}(\gamma, p_0)$ data.

The results are shown in Table III where the coefficients in parentheses are smaller than the errors and are assumed to be zero for the present discussion. The results indicate that the main mode of interaction in the photodisintegration of ${}^9\text{Be}$ is an overlap of $E1$ and $E2$ plus $E1/E2$ interference in the case of (γ, p_0) and $E1$ plus $E1/E2$ interference in the cases of (γ, d_{0+1}) and (γ, t_0) . The angular distributions provide information on the corresponding states and reaction mechanisms. These results will be discussed later for the relevant reactions.

The ${}^9\text{Be}(\gamma, p_{0+1})$ cross section measurement by Denisov and Kul'chitskii [16] is compared in Fig. 7. Their results, which include an unknown p_1 contribution, agree with the present (γ, p_0) results near 22 MeV, but are about twice the present results near 27 MeV. From the present proton energy distribution shown in Fig. 3, the excess yield of p_1 is obscured by the p_0 contribution. This indicates that the (γ, p_1) cross section is much smaller than the (γ, p_0) cross section at $E_\gamma = 24$ and 26 MeV. Therefore the discrepancy between the present result and that of Denisov and Kul'chitskii does not seem to be due to the (γ, p_1) contribution. The method reported here has been used to determine (γ, p_0) cross sections for many other nuclei and gives agreement with the already established data.

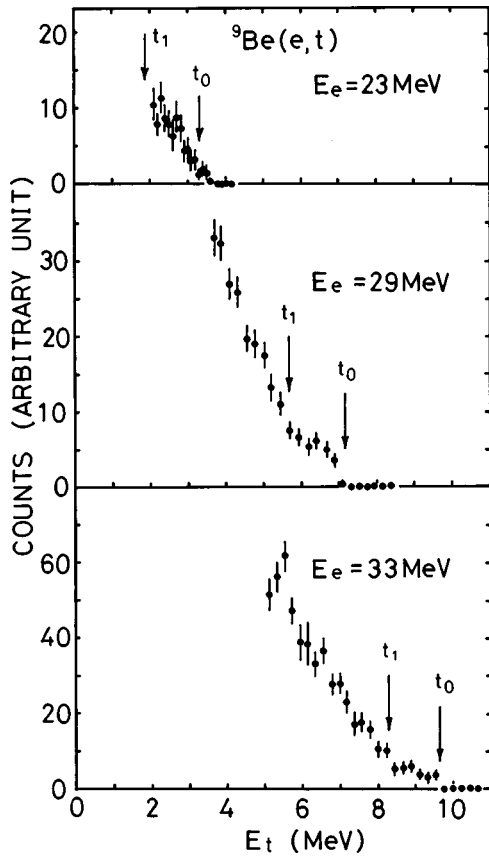


FIG. 5. Example of triton energy distributions by electron bombardment. The end-point energies of t_0 and t_1 are indicated by arrows.

In the case of ${}^9\text{Be}(\gamma, d_{0+1})$ shown in Fig. 8, the results of Denisov and Kul'chitskii are similar to the present results except that the structures around 28 MeV are much stronger. The cross section of Denisov and Kul'chitskii for (γ, t_0) is about 1.5 times the present result as shown in Fig. 9. Despite the fact that the present detection angle is 125° while that of Ref. [16] is 90° , consideration of the angular distribution shown in Figs. 11–13 suggests that this discrepancy is not due to the difference in the detection angle.

The photodisintegration cross sections for ${}^9\text{Be}$ are shown in Fig. 14(a) where vertical bars show the photoabsorption cross section [10] together with (γ, n) (solid curve) [13], (γ, p) (histogram) [12], (γ, p_0) (open circles), (γ, d_{0+1}) (open triangles), (γ, t_0) (solid circles), $(\gamma, {}^3\text{He}_0)$ (crosses). The last four cross sections are the present results derived from $d\sigma/d\Omega$ at 125° multiplied by 4π . The uncertainty in this assumption will be less than 10% with an angular distribution similar to that shown in Table III. The present data are also shown magnified in Fig. 14(b).

Denisov and Kul'chitskii [16] also measured the (γ, p) cross section using the photon difference method and obtained a cross section that was about half the absolute cross section reported in previous measurements using the same method [12,21]. The (γ, p) result of Denisov and Kul'chitskii is approximately equal to the (γ, p_0) cross section presented here and a little smaller than the (γ, p_{0+1}) cross section reported in the same paper. When the sum of the (γ, n) and (γ, p) cross sections is compared with the total photon absorption cross section, reasonable agreement is

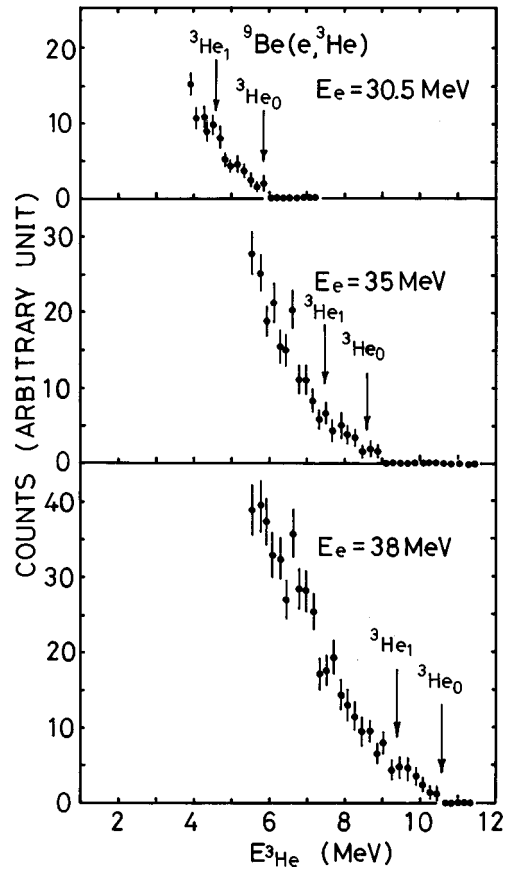


FIG. 6. Example of ${}^3\text{He}$ energy distributions by electron bombardment. The end-point energies of ${}^3\text{He}_0$ and ${}^3\text{He}_1$ are indicated by arrows.

only possible if the (γ, p) cross section reported by Cliekmann *et al.* [12] is used in the sum rather than that of Denisov and Kul'chitskii. This is included in Fig. 14(a).

Calculations of the photonuclear cross section in the giant dipole resonance (GDR) region of $1p$ shell nuclei, including ${}^6\text{Li}$, ${}^7\text{Li}$, ${}^9\text{Be}$, and others, have been made by Ishkhanov *et al.* These were based on supermultiplet structure in the shell model [22]. The results show configuration splitting depending on the shell of the initial nucleon. Experimental photoabsorption cross sections of these nuclei agree approximately with these theoretical results. In particular, the strength at high energies in the GDR corresponds to excitation of the nucleon from the $1s_{1/2}$ shell. They raised the possibility that this group results from cluster effects.

The giant resonances for ${}^9\text{Be}(\gamma, n)$ and ${}^9\text{Be}(\gamma, p)$ shown in Fig. 14 are similar. The photoneutron yield in this energy region predominantly involves excitation of the ${}^8\text{Be}$ core as mentioned before. This suggests that the photoprotons are emitted from the ${}^8\text{Be}$ core in ${}^9\text{Be}$, which is the analog of the (γ, n) reaction leaving residual states higher than 16.6 MeV in ${}^8\text{Be}$.

The (γ, p) cross section integrated from 18 to 37 MeV is about 0.6 times the (γ, n) cross section. The cross sections for ${}^4\text{He}(\gamma, n)$ and ${}^4\text{He}(\gamma, p)$ as studied by many experiments [23] are approximately equal except for several MeV above the threshold. However, the ratio of 0.6 in the high-energy region and also the fact that this ratio decreases in the higher-energy region cannot be explained by the Coulomb effect.

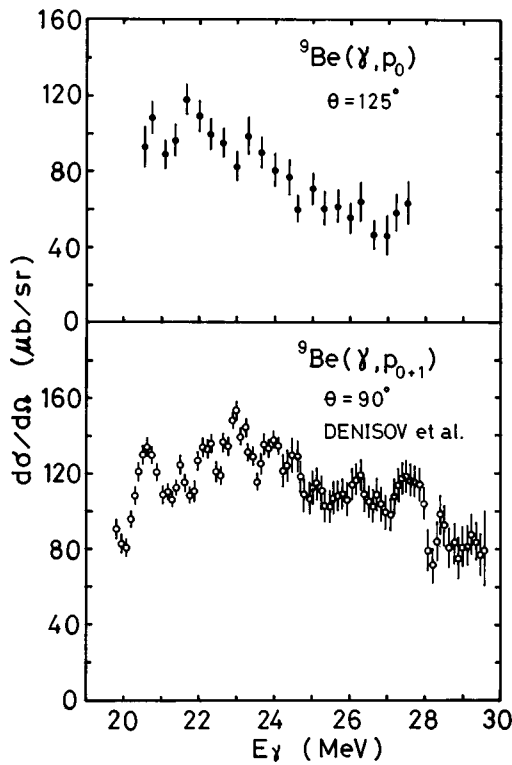


FIG. 7. Cross section of ${}^9\text{Be}(\gamma, p_0)$. Solid circles, present result at $\theta = 125^\circ$. Open circles, Denisov *et al.* ${}^9\text{Be}(\gamma, p_{0+1})$ at $\theta = 90^\circ$ [16].

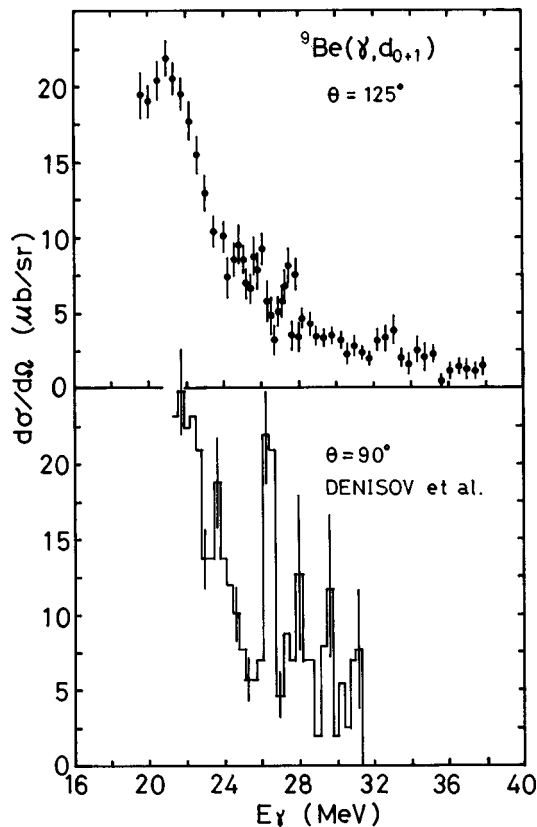


FIG. 8. Cross section of ${}^9\text{Be}(\gamma, d_{0+1})$. Solid circles, present result at $\theta = 125^\circ$. Histogram, Denisov *et al.* at $\theta = 90^\circ$ [16].

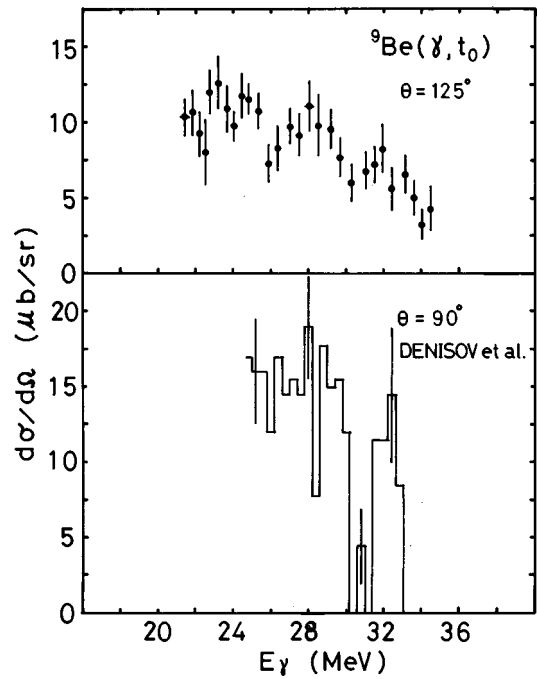


FIG. 9. Cross section of ${}^9\text{Be}(\gamma, t_0)$. Solid circles, present result at $\theta = 125^\circ$. Histogram, Denisov *et al.* at $\theta = 90^\circ$ [16].

This shows that some modification of the present simple transition models is necessary. Although some explanation of the difference may be possible in terms of isospin as mentioned later, the explanation of this ratio is currently an open question.

The cross sections for ${}^9\text{Be}(\gamma, d_{0+1})$, ${}^9\text{Be}(\gamma, t_0)$, and ${}^9\text{Be}(\gamma, {}^3\text{He}_0)$ have similar strengths and are about one order of magnitude smaller than the ${}^9\text{Be}(\gamma, p_0)$ cross section. The ${}^9\text{Be}(\gamma, d_{0+1})$ cross section shows a strong peak from the threshold region up to around 26 MeV, but above this it is relatively flat. This is in contrast to the cross sections for ${}^9\text{Be}(\gamma, t_0)$ and ${}^9\text{Be}(\gamma, {}^3\text{He}_0)$. The ${}^9\text{Be}(\gamma, t_0)$ and ${}^9\text{Be}(\gamma, {}^3\text{He}_0)$ cross sections are similar.

The cluster model has been successfully applied to light nuclei. Nuclei with fewer than eight nucleons are well described by a two-cluster model using, among others, the resonating group method (RGM) as summarized in the review article in [24]. However, for nuclei with more than

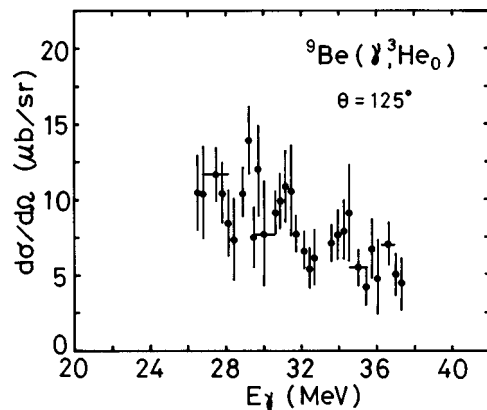


FIG. 10. Cross section of ${}^9\text{Be}(\gamma, {}^3\text{He}_0)$. Solid circles, present result at $\theta = 125^\circ$. Horizontal lines show the energy resolution.

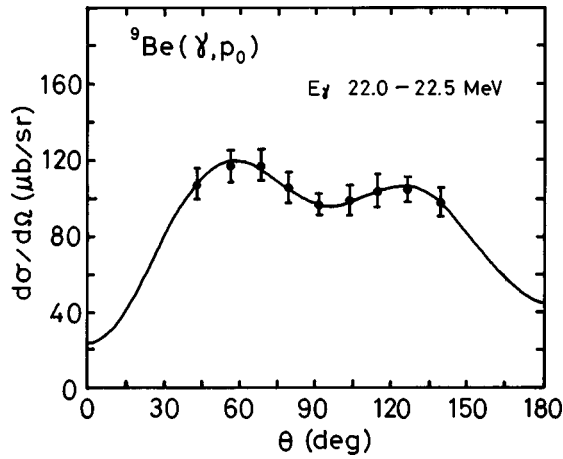


FIG. 11. Angular distribution of ${}^9\text{Be}(\gamma, p_0)$ ranging from 22.0 to 22.5 MeV. The curve is the result of the χ^2 fitting shown in Table III.

eight nucleons, the model usually involves three or more clusters, and calculations are tedious. However, they can be done using the generator coordinate method (GCM) [25], for example.

Experimental results for photodisintegration of ${}^6\text{Li}$ and ${}^7\text{Li}$ have been compared with two-cluster model calculations. For ${}^9\text{Be}$, experimental studies have been made of the total photoabsorption cross section, the (γ, n) cross section, and also charged particle photodisintegration, but theoretical analyses are few.

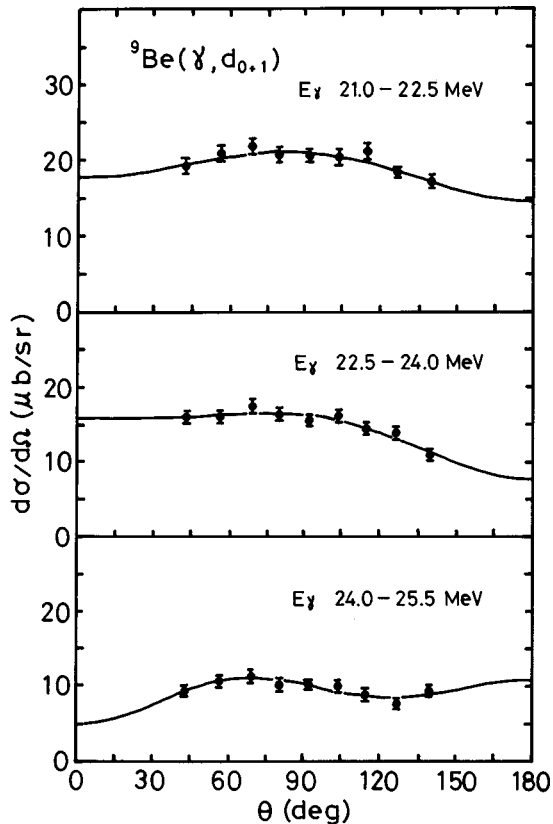


FIG. 12. Angular distribution of ${}^9\text{Be}(\gamma, d_{0+1})$ ranging from 21.0 to 22.5 MeV, from 22.5 to 24.0 MeV, and from 24.0 to 25.5 MeV. The curves are the results of the χ^2 fitting shown in Table III.

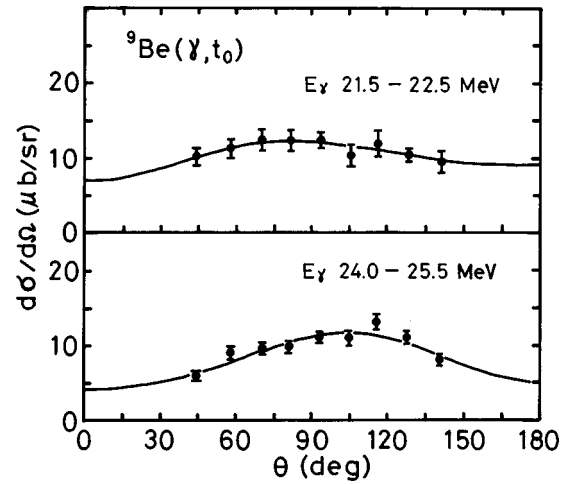


FIG. 13. Angular distribution of ${}^9\text{Be}(\gamma, t_0)$ ranging from 21.5 to 22.5 MeV and from 24.0 to 25.5 MeV. The curves are the result of the χ^2 fitting shown in Table III.

Many particle shell model calculations have been made of the photoabsorption cross section of ${}^9\text{Be}$ by Majling *et al.* [26], Shackleton [26], and Ishkhanov *et al.* [22]. They employed different residual interactions between all nine nucleons. Their results reproduce some structures seen weakly in the experimental (γ, n) cross section. The measured cross section above 30 MeV is still large, and although Majling *et al.* predict a large cross section in the high-energy region, their calculation cannot reproduce the cross section from threshold to 18 MeV. The result of Shackleton does not show any significant cross section in the high-energy region. Ishkhanov *et al.* successfully reproduced the energy and intensity dependence of the experimental broad cross section for $1p$ shell nuclei by configuration splitting due to supermultiplet structure for $E1$ transitions from the $1p$ valence nucleon and the $1s$ core. The result of their calculation on ${}^9\text{Be}(\gamma, n)$ shows that the strongest channels lead to the population of states of the ${}^8\text{Be}$ nucleus beginning at 16.6 MeV, where the emission of fragments from the ${}^8\text{Be}$ core is more important.

Two-cluster model calculations for the photodisintegration of ${}^6\text{Li}$ and ${}^7\text{Li}$ have been made with less ambiguity, and the results agree well with the experimental data [4,5]. However, no theoretical cluster model calculation has been made for the photodisintegration of ${}^9\text{Be}$. Qualitative analyses using the cluster model will be discussed here for photodisintegration of ${}^9\text{Be}$ in comparison with the cases of ${}^6\text{Li}$ and ${}^7\text{Li}$ for which there are many cluster model calculations.

In the present qualitative discussion, the crude assumption is made that the cluster can be assumed to be free in the

TABLE II. Theoretical angular distribution for photonuclear reactions assuming compound process. The results are given for the multipolarity $E1, E2$, and their interference for the reaction.

Interaction mode	$d\sigma/d\Omega$
$E1$	$A_0[P_0(\cos \theta) + a_2P_2(\cos \theta)]$
$E2$	$A_0[P_0(\cos \theta) + a_2P_2(\cos \theta) + a_4P_4(\cos \theta)]$
Interference	
$E1-E2$	$A_0[a_1P_1(\cos \theta) + a_3P_3(\cos \theta)]$

TABLE III. Angular distribution coefficients a_i determined by a χ^2 fit with experimental results by Eq. (4). The coefficients in parentheses are smaller than the errors and are assumed to be zero for estimation of main modes.

E_γ (MeV)	A_0 ($\mu\text{b}/\text{sr}$)	a_1	a_2	a_3	a_4	Main mode ^a
			⁹ Be(γ, p_0) ^b			
22.0–22.5	127 \pm 3	(0.02 \pm 0.04)	-0.22 \pm 0.12	-0.11 \pm 0.09	-0.28 \pm 0.09	E1, E2, E1-E2
			⁹ Be(γ, d_{0+1}) ^c			
21.0–22.5	19.4 \pm 0.4	0.08 \pm 0.06	-0.17 \pm 0.06	(0.01 \pm 0.10)		E1, E1-E2
22.5–24.0	14.9 \pm 0.3	0.21 \pm 0.06	0.20 \pm 0.06	(0.06 \pm 0.10)		E1, E1-E2
24.0–25.5	9.6 \pm 0.3	(-0.02 \pm 0.08)	-0.62 \pm 0.31	-0.28 \pm 0.13		E1, E1-E2
			⁹ Be(γ, t_0) ^c			
21.5–22.5	10.9 \pm 0.5	(-0.01 \pm 0.13)	-0.26 \pm 0.13	(-0.10 \pm 0.21)		E1
24.0–25.5	9.2 \pm 0.3	-0.20 \pm 0.08	-0.48 \pm 0.11	0.15 \pm 0.14		E1, E1-E2

^aMain mode indicates the possible modes on E1, E2 interactions and their interference deduced from the present results of a_i . E1-E2 means interference between E1 and E2.

^bEquation (4) is taken up to $i=4$ for χ^2 fitting.

^cEquation (4) is taken up to $i=3$ for χ^2 fitting.

binding potential. For this approximation, Table IV lists the possible cluster configurations of the target and residual states for the cases of ⁶Li, ⁷Li, and ⁹Be. In the table, the relevant residual configuration resulting from the cluster knockout is underlined. The number of the possible cluster transitions in ⁹Be is much greater than for ⁶Li and ⁷Li.

In order to maintain a consistent discussion, consideration of the residual states is limited to the ground state when the model is compared with the experimental results for the (γ, p_0), (γ, d_0), (γ, t_0), and ($\gamma, ^3\text{He}_0$) reactions. For (γ, n) and (γ, p) reactions, residual excited states are included. The cluster structure for light nuclei with more than four nucleons is discussed in Ref. [24]. The cluster transitions given in Table IV are selected so that the main cluster configurations in both the target and residual nuclei agree with a component of the configuration in Ref. [24]. The results of such transitions are shown in Table V, where the cluster configurations for the residual states are also indicated. When the cluster configuration of the excited state has already been defined from experiment, it is shown by “ex.s.,” and it is assumed that one of the component clusters in this configuration is directly emitted from the excited states following photoexcitation.

In the cluster model, photodisintegration involves two types of transitions by the component clusters in the target ground state. One is direct knockout of a cluster, and the other is based on the photodisintegration of a component cluster. The knockout process for a two-cluster system has been calculated in the microscopic potential model and by the RGM. Most recently, Dubovichenko and Dzhazairov-Kakhramanov have calculated the photonuclear process for ⁶Li using a cluster model via the channels [$\alpha \cdot d$], [$^3\text{He} \cdot t$], and [$^5\text{Li} \cdot n$] [4]. The calculation was based on microscopic potentials with forbidden states and was compared with experimental cross sections for ⁶Li(γ, d), ⁶Li(γ, t), ⁶Li(γ, n), and the relevant inverse reactions. The agreement between theory and experiment was generally good. In the case of ⁶Li(γ, t), the comparison was difficult because of poor experimental data. They also applied the same method to ⁷Li

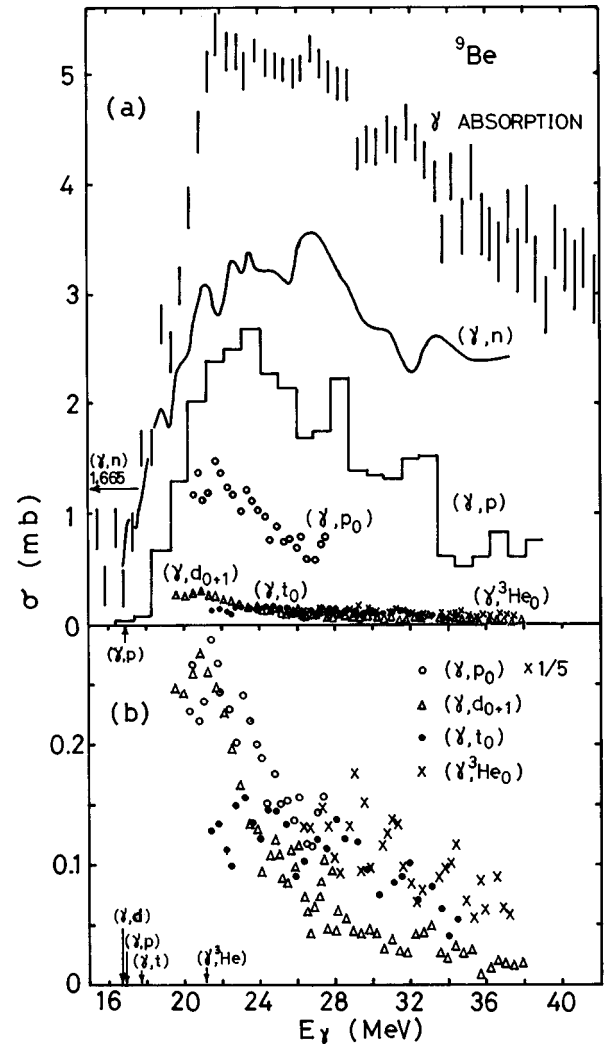


FIG. 14. (a) Cross sections for photodisintegration of ⁹Be ($E_\gamma \geq 16$ MeV). Threshold energies are shown by arrows. Vertical bars, photoabsorption cross section [10]; solid curve, (γ, n) [13]; histogram, (γ, p) [12]; open circles, (γ, p_0) present data; open triangles, (γ, d_{0+1}) present data; solid circles, (γ, t_0) present data; crosses, ($\gamma, ^3\text{He}_0$) present data. (b) Magnified figure of (γ, p_0), (γ, d_{0+1}), (γ, t_0), and ($\gamma, ^3\text{He}_0$), the same as in (a).

TABLE IV. Possible cluster configuration for photodisintegration of ${}^6\text{Li}$, ${}^7\text{Li}$, and ${}^9\text{Be}$. An underline shows the result by cluster knockout reaction.

Reaction	(γ, n)	(γ, p)	(γ, d)	(γ, t)	$(\gamma, {}^3\text{He})$
Target nucleus			Residual nucleus		
${}^6\text{Li}$	${}^5\text{Li}$	${}^5\text{He}$	${}^4\text{He}$	${}^3\text{He}$	${}^3\text{H}$
$\alpha \cdot d$	$\alpha \cdot p$	$\alpha \cdot n$	$\underline{\alpha}$		
	${}^3\text{He} \cdot d$	$t \cdot d$	$d \cdot d$	$p \cdot d$	$n \cdot d$
${}^3\text{He} \cdot t$	${}^3\text{He} \cdot d$	${}^3\text{He} \cdot 2n$	${}^3\text{He} \cdot n$	$\underline{{}^3\text{He}}$	
	$2p \cdot t$	$d \cdot t$	$p \cdot t$		\underline{t}
${}^5\text{He} \cdot p^a$		${}^5\text{He}^a$			
	$\alpha \cdot p$	${}^4\text{H} \cdot p^b$	$t \cdot p$	$d \cdot p$	$2n \cdot p$
${}^5\text{Li} \cdot n^c$	${}^5\text{Li}^c$				
	${}^4\text{Li} \cdot n^d$	$\alpha \cdot n$	${}^3\text{He} \cdot n$	$2p \cdot n$	$d \cdot n$
${}^7\text{Li}$	${}^6\text{Li}$	${}^6\text{He}$	${}^5\text{He}$	${}^4\text{He}$	${}^4\text{H}$
$\alpha \cdot t$	$\alpha \cdot d$	$\alpha \cdot 2n$	$a \cdot n$	$\underline{\alpha}$	
	${}^3\text{He} \cdot t$	$t \cdot t$	$d \cdot t$	$p \cdot t$	$n \cdot t$
${}^3\text{He} \cdot {}^4\text{H}^b$	${}^3\text{He} \cdot t$	${}^3\text{He} \cdot 3n$	${}^3\text{He} \cdot 2n$	${}^3\text{He} \cdot n$	
	$2p \cdot {}^4\text{H}^b$	$d \cdot {}^4\text{H}^b$	$p \cdot {}^4\text{H}^b$		$\underline{{}^4\text{H}^b}$
${}^5\text{He} \cdot d^a$	${}^5\text{He} \cdot p^a$	${}^5\text{He} \cdot n^a$	${}^5\text{He}^a$		
	$\alpha \cdot d$	${}^4\text{H} \cdot d^b$	$t \cdot d$	$d \cdot d$	$2n \cdot d$
${}^5\text{Li} \cdot 2n^c$	${}^5\text{Li} \cdot n^c$				
	${}^4\text{Li} \cdot 2n^d$	$\alpha \cdot 2n$	${}^3\text{He} \cdot 2n$	$2p \cdot 2n$	$d \cdot 2n$
${}^6\text{He} \cdot p^e$		${}^6\text{He}^e$			
	${}^5\text{He} \cdot p^a$	${}^5\text{H} \cdot p^f$	${}^4\text{H} \cdot p^b$	$t \cdot p$	$3n \cdot p$
${}^6\text{Li} \cdot n$	${}^6\text{Li}$				
	${}^5\text{Li} \cdot n^c$	${}^5\text{He} \cdot n^a$	$\alpha \cdot n$	${}^3\text{He} \cdot n$	$t \cdot n$
${}^9\text{Be}$	${}^8\text{Be}$	${}^8\text{Li}$	${}^7\text{Li}$	${}^6\text{Li}$	${}^6\text{He}$
$\alpha \cdot \alpha \cdot n$	$\underline{\alpha \cdot \alpha}$				
	$\alpha \cdot {}^3\text{He} \cdot n$	$\alpha \cdot t \cdot n$	$\alpha \cdot d \cdot n$	$\alpha \cdot p \cdot n$	$\alpha \cdot n \cdot n$
$\alpha \cdot t \cdot d$	$\alpha \cdot t \cdot p$	$\alpha \cdot t \cdot n$	$\underline{\alpha \cdot t}$		
	$\alpha \cdot d \cdot d$	$\alpha \cdot 2n \cdot d$	$\underline{\alpha \cdot n \cdot d}$	$\underline{\alpha \cdot d}$	
	${}^3\text{He} \cdot t \cdot d$	$t \cdot t \cdot d$	$d \cdot t \cdot d$	$p \cdot t \cdot d$	$n \cdot t \cdot d$
$\alpha \cdot p \cdot {}^4\text{H}^b$	$\alpha \cdot p \cdot t$	$\alpha \cdot p \cdot 3n$	$\alpha \cdot p \cdot 2n$	$\alpha \cdot p \cdot n$	
		$\underline{\alpha \cdot {}^4\text{H}^b}$			
	${}^3\text{He} \cdot p \cdot {}^4\text{H}^b$	$t \cdot p \cdot {}^4\text{H}^b$	$d \cdot p \cdot {}^4\text{H}^b$	$p \cdot p \cdot {}^4\text{H}^b$	$n \cdot p \cdot {}^4\text{H}^b$
${}^3\text{He} \cdot t \cdot t$	${}^3\text{He} \cdot t \cdot d$	${}^3\text{He} \cdot t \cdot 2n$	${}^3\text{He} \cdot t \cdot n$	$\underline{{}^3\text{He} \cdot t}$	
	$2p \cdot t \cdot t$	$d \cdot t \cdot t$	$p \cdot t \cdot t$		$\underline{t \cdot t}$
${}^3\text{He} \cdot d \cdot {}^4\text{H}^b$	${}^3\text{He} \cdot d \cdot t$	${}^3\text{He} \cdot d \cdot 3n$	${}^3\text{He} \cdot d \cdot 2n$	${}^3\text{He} \cdot d \cdot n$	
	${}^3\text{He} \cdot p \cdot {}^4\text{H}^b$	${}^3\text{He} \cdot n \cdot {}^4\text{H}^b$	$\underline{{}^3\text{He} \cdot {}^4\text{H}^b}$		
	$2p \cdot d \cdot {}^4\text{H}^b$	$d \cdot d \cdot {}^4\text{H}^b$	$p \cdot d \cdot {}^4\text{H}^b$		$\underline{d \cdot {}^4\text{H}^b}$
${}^5\text{He} \cdot \alpha^a$	${}^5\text{He} \cdot {}^3\text{He}^a$	${}^5\text{He} \cdot t^a$	${}^5\text{He} \cdot d^a$	${}^5\text{He} \cdot p^a$	${}^5\text{He} \cdot n^a$
	$\alpha \cdot \alpha$	${}^4\text{H} \cdot \alpha^b$	$t \cdot \alpha$	$d \cdot \alpha$	$2n \cdot \alpha$
${}^5\text{Li} \cdot {}^4\text{H}^{c,b}$	${}^5\text{Li} \cdot t^c$	${}^5\text{Li} \cdot 3n^c$	${}^5\text{Li} \cdot 2n^c$	${}^5\text{Li} \cdot n^c$	
	${}^4\text{Li} \cdot {}^4\text{H}^{d,b}$	$\alpha \cdot {}^4\text{H}^b$	${}^4\text{He} \cdot {}^4\text{H}^b$	$2p \cdot {}^4\text{H}^b$	$d \cdot {}^4\text{H}^b$
${}^6\text{He} \cdot {}^3\text{He}^e$	${}^6\text{He} \cdot 2p^e$	${}^6\text{He} \cdot d^e$	${}^6\text{He} \cdot p^e$		$\underline{{}^6\text{He}^e}$
	${}^5\text{He} \cdot {}^3\text{He}^a$	${}^5\text{H} \cdot {}^3\text{He}^f$	${}^4\text{H} \cdot {}^3\text{He}^b$	$t \cdot {}^3\text{He}$	$3n \cdot {}^3\text{He}$
${}^6\text{Li} \cdot t$	${}^6\text{Li} \cdot d$	${}^6\text{Li} \cdot 2n$	${}^6\text{Li} \cdot n$	$\underline{{}^6\text{Li}}$	
	${}^5\text{Li} \cdot t^c$	${}^5\text{He} \cdot t^a$	$\alpha \cdot t$	${}^4\text{He} \cdot t$	$t \cdot t$
${}^7\text{Li} \cdot d$	${}^7\text{Li} \cdot d$	${}^7\text{Li} \cdot n$	${}^7\text{Li}$		
	${}^6\text{Li} \cdot d$	${}^6\text{He} \cdot d^e$	$\underline{{}^5\text{He} \cdot d^a}$	$\alpha \cdot d$	${}^4\text{H} \cdot d^b$

^a ${}^5\text{He}$ may be $\alpha \cdot n$, $t \cdot d$, and $p \cdot {}^4\text{H}$.

^b ${}^4\text{H}$ may be $t \cdot n$ and $d \cdot 2n$.

^c ${}^5\text{Li}$ may be $\alpha \cdot p$, ${}^3\text{He} \cdot d$, and $t \cdot 2p$.

^d ${}^4\text{Li}$ may be ${}^3\text{He} \cdot p$ and $d \cdot 2p$.

^e ${}^6\text{He}$ may be $\alpha \cdot 2n$, ${}^3\text{He} \cdot 3n$, $t \cdot t$, $d \cdot {}^4\text{H}$, and $p \cdot {}^5\text{H}$.

^f ${}^5\text{H}$ may be $t \cdot 2n$.

TABLE V. Expected transition of the main cluster for photodisintegration of ${}^6\text{Li}$, ${}^7\text{Li}$, and ${}^9\text{Be}$. The elementary reaction on a cluster component is shown, and knockout of a cluster component is indicated by \rightarrow . Cluster configuration is shown by []. The residual configuration is selected so as to be the ground state except (γ, n) in which excited residual states are included. The threshold energy is shown following the residual nucleus.

Reaction	(γ, n)	(γ, p_0)	(γ, d_0)	(γ, t_0)	$(\gamma, {}^3\text{He}_0)$	
Target nucleus	Residual nucleus		Threshold energy (MeV)			
[Main cluster configuration] ^a	Transition of main cluster component					
	[Residual cluster configuration] ^a					
	${}^6\text{Li}$	${}^5\text{Li}$ 5.67	${}^5\text{He}$ 4.59	${}^4\text{He}$ 1.48	${}^3\text{He}$ 15.80	${}^3\text{H}$ 15.80
g.s.	$[\alpha \cdot d]$	$d \rightarrow p + n$	$d \rightarrow n + p$	$d \rightarrow$		
	$[{}^5\text{Li} \cdot n]$	$[\alpha \cdot p]$	$[\alpha \cdot n]$	$[\alpha]$		
	$[{}^5\text{He} \cdot p]$	$\alpha \rightarrow {}^3\text{He} + n$	$\alpha \rightarrow t + p$	$\alpha \rightarrow d + d$	$\alpha \rightarrow p + t$	$\alpha \rightarrow n + {}^3\text{He}$
		$[{}^3\text{He} \cdot d]$	$[t \cdot d]$	$[d \cdot d]$	$[p \cdot d]$	$[n \cdot d]$
		$n \rightarrow$	$p \rightarrow$			
		$[{}^5\text{Li}]$	$[{}^5\text{He}]$			
ex.s.	$[{}^3\text{He} \cdot t]$			$t \rightarrow$	${}^3\text{He} \rightarrow$	
				$[{}^3\text{He}]$	$[t]$	
	${}^7\text{Li}$	${}^6\text{Li}$ 7.25	${}^6\text{He}$ 9.98	${}^5\text{He}$ 9.62	${}^4\text{He}$ 2.47	${}^4\text{H}$ 31.52
g.s.	$[\alpha \cdot t]$	$t \rightarrow d + n$	$t \rightarrow 2n + p$	$t \rightarrow n + d$	$t \rightarrow$	
	$[{}^6\text{Li} \cdot n]$	$[\alpha \cdot d]$	$[\alpha \cdot 2n]$	$[\alpha \cdot n]$	$[\alpha]$	
	$[{}^6\text{Li}^* \cdot n]$	$\alpha \rightarrow {}^3\text{He} + n$		$\alpha \rightarrow d + d$	$\alpha \rightarrow p + t$	$\alpha \rightarrow n + {}^3\text{He}$
	$[{}^5\text{He} \cdot d]$	$[{}^3\text{He} \cdot t]$		$[d \cdot t]$	$[p \cdot t]$	$[n \cdot t]$
	${}^9\text{Be}$	${}^8\text{Be}$ 1.67	${}^8\text{Li}$ 16.89	${}^7\text{Li}$ 16.70	${}^6\text{Li}$ 17.69	${}^6\text{He}$ 21.18
g.s.	$[\alpha \cdot \alpha \cdot n]$	$n \rightarrow$				
		$[\alpha \cdot \alpha]$				
		$\alpha \rightarrow {}^3\text{He} + n$	$\alpha \rightarrow t + p$	$\alpha \rightarrow d + d^c$	$\alpha \rightarrow p + t^d$	$\alpha \rightarrow n + {}^3\text{He}$
		$[\alpha \cdot {}^3\text{He} \cdot n]$	$[\alpha \cdot t \cdot n]$	$[\alpha \cdot d \cdot n]$	$[\alpha \cdot p \cdot n]$	$[\alpha \cdot n \cdot n]$
ex.s.	$[{}^5\text{He} \cdot \alpha]$					

^aDominant cluster configuration of the ground state is taken as follows (when the excited state is shown, it is indicated by ex.s.): ${}^3\text{H}$: $[n \cdot d]$. ${}^3\text{He}$: $[p \cdot d]$. ${}^4\text{H}$: $[n \cdot t]$. ${}^4\text{He}$: $[t \cdot p]$, $[{}^3\text{He} \cdot n]$, weak $[d \cdot d]$ [27]. ${}^5\text{He}$: $[t \cdot d]$, $[\alpha \cdot n]$ [24]. ${}^5\text{Li}$: $[\alpha \cdot p]$, $[{}^3\text{He} \cdot d]$ [24]. ${}^6\text{He}$: $[\alpha \cdot 2n]$ [24]. ${}^6\text{Li}$: $[\alpha \cdot d]$, rather mild effect of $[{}^5\text{Li} \cdot n]$ and $[{}^5\text{He} \cdot p]$ [24]. ${}^6\text{Li}$ ex.s.: $[\alpha \cdot d]$, $[{}^3\text{He} \cdot t]$ [24]. ${}^7\text{Li}$: $[\alpha \cdot t]$, additional configuration of $[{}^6\text{Li} \cdot n]$, $[{}^6\text{Li} \cdot n^*]$, and $[{}^5\text{He} \cdot d]$ for good description [24]. ${}^7\text{Li}$ ex.s. (<50 MeV): $[\alpha \cdot t]$ [24]. ${}^8\text{Li}$: $[\alpha \cdot t \cdot n]$, $[n \cdot {}^7\text{Li}]$ [24]. ${}^8\text{Be}$: $[\alpha \cdot \alpha]$ [24]. ${}^8\text{Be}$ ex.s.: $[\alpha \cdot \alpha]$, $[\alpha \cdot \alpha^*]$ [24]. ${}^9\text{Be}$: most important for $[\alpha \cdot \alpha \cdot n]$ [24]. ${}^9\text{Be}$ ex.s.: $[{}^5\text{He} \cdot \alpha]$ [24].

^bThese configurations are neglected for transition, though they are necessary for a detailed discussion for ${}^7\text{Li}$.

^c $[\alpha \cdot d \cdot n]$ may be approximated to $[{}^6\text{Li} \cdot n]$.

^d $[\alpha \cdot p \cdot n]$ may be approximated to $[{}^5\text{Li} \cdot n]$.

through the $[\alpha \cdot t]$ channel and obtained good agreement with the experimental cross sections for both ${}^7\text{Li}(\gamma, \alpha)$ and the inverse reaction [5].

Sketches of the experimental cross sections for (γ, n) , (γ, p_0) , (γ, d_0) , (γ, t_0) , and $(\gamma, {}^3\text{He}_0)$ on ${}^6\text{Li}$, ${}^7\text{Li}$, and ${}^9\text{Be}$ are shown in Fig. 15. Also shown are the cross sections by the same decays for ${}^2\text{H}$, ${}^3\text{H}$, ${}^3\text{He}$, and ${}^4\text{He}$, so that comparison can be made in discussing the assumption of disintegration of free cluster. The cross section of ${}^9\text{Be}(\gamma, d_{0+1}){}^7\text{Li}$ is taken to be $\sigma(\gamma, d_0)$, because the cluster configuration may be the same for the ground and first excited states in ${}^7\text{Li}$.

If a target nucleus A (mass A) is described by the configuration of the cluster C_i [mass C_i ($i=1 \sim N$)], mass A is given by $\sum_i C_i$ plus the binding energy of the clusters. Consider that the reaction $A(\gamma, x)B$ which emits a particle x

(mass x) results from the elementary reaction $C_s + \gamma = D_s + x$. If the ground state of the residual nucleus B_0 (mass B_0) is described by the sum of the free cluster mass C_i ($i \neq s$) and D_s plus the binding energy of the clusters, the threshold energy of the reaction $A(\gamma, x_0)B_0$ is given by $E(\gamma, x_0; C_s \rightarrow D_s + x) = B_0 + x - A$, which does not depend on the elementary reaction threshold for any kind of component cluster C_s .

The following qualitative discussion for ${}^9\text{Be}$ and also for ${}^6\text{Li}$ and ${}^7\text{Li}$ as a check, will consider the elementary reactions. In this discussion, processes involving knockout of a cluster from the ground state and ejection of a cluster that exists in the configuration of a highly excited state are assumed to be far more likely than the elementary reaction on the component cluster in the ground state.

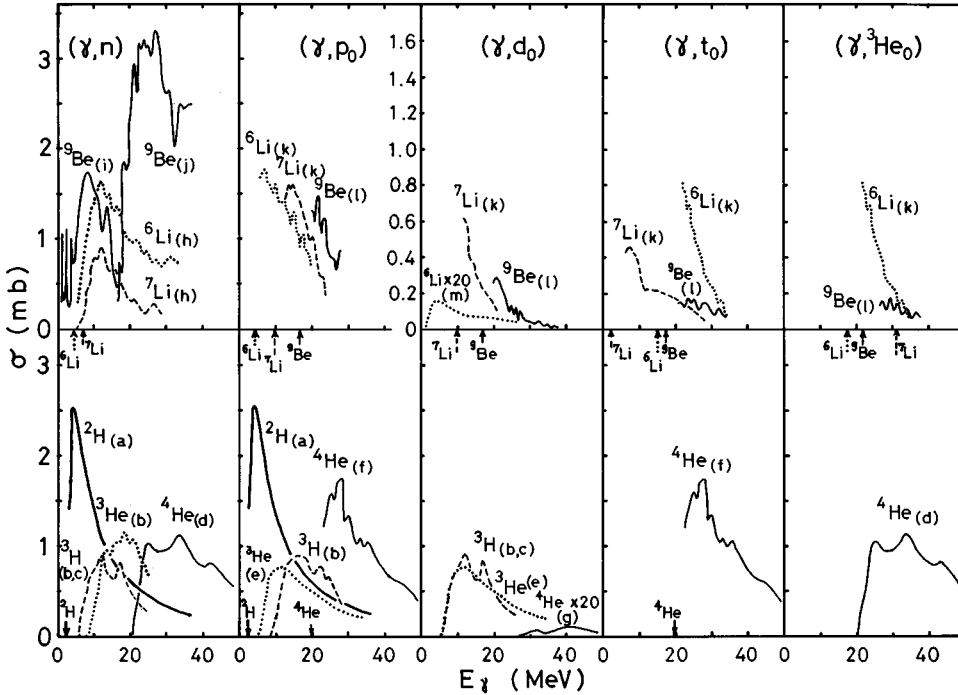


FIG. 15. Comparison of the experimental cross sections of (γ, n) , (γ, p_0) , (γ, d_0) , (γ, t_0) , and $(\gamma, {}^3\text{He}_0)$ on ${}^2\text{H}$, ${}^3\text{H}$, ${}^3\text{He}$, ${}^4\text{He}$, ${}^6\text{Li}$, ${}^7\text{Li}$, and ${}^9\text{Be}$. Arrows show threshold energies in the cases that they are not found from the cross section. References (a) [28], (b) [29], (c) [30], (d) [31], (e) [32], (f) [33], (g) [34], (h) [35], (i) [17], (j) [13], (k) [36], (l) present result, and (m) [37].

A. (γ, n) and (γ, p) cross sections leaving all the residual states

The cluster configuration contributing in ${}^9\text{Be}$ is $[\alpha \cdot \alpha \cdot n]$ as shown in Table V. Knockout of a neutron leaves the ground and low-lying residual states ($T=0$) of ${}^8\text{Be}$. In addition, the elementary reaction involving neutron emission from an α cluster may lead to $T=1$ states. The knockout process leads to the (γ, n) cross section in the low-energy region just above threshold (the so-called pygmy giant resonance) as shown in Fig. 15. The ${}^9\text{Be}(\gamma, p){}^8\text{Li}$ reaction leaving the residual nucleus in low-lying states ($T=1$) can only be described by the elementary reaction ${}^4\text{He}(\gamma, p){}^3\text{H}$. This (γ, p) reaction is the analog of the ${}^9\text{Be}(\gamma, n){}^8\text{Be}$ reaction which leaves the $T=1$ states resulting from the elementary reaction ${}^4\text{He}(\gamma, n){}^3\text{He}$. The residual state populated in this ${}^9\text{Be}(\gamma, n){}^8\text{Be}$ reaction is the analog of the low-lying state in ${}^8\text{Li}(T=1)$ left by the (γ, p) reaction. Since the lowest analog state is at 16.6 MeV in ${}^8\text{Be}$, the (γ, n) reaction based on this elementary reaction appears in a region of energy higher than 16.6 MeV above the ${}^9\text{Be}(\gamma, n)$ threshold of 1.665 MeV, namely, at 18.3 MeV. Neutron decay from this mode reproduces the experimental results which show population of residual states at 16.6 MeV [38]. A large giant resonance in the (γ, n) and (γ, p) reactions at energies above 18 MeV, as shown in Figs. 14 and 15, involves mainly the elementary reaction of an α cluster.

The value of 0.6 for the ratio of the ${}^9\text{Be}(\gamma, p)$ cross section to the ${}^9\text{Be}(\gamma, n)$ cross section is an open question as mentioned before. One possible influence on this ratio is a strong channel for neutron emission by knockout of a neutron via $T=1/2$ states, leaving the $T=0$ residual states in ${}^8\text{Be}$. This corresponds to the extension of the pygmy resonance into a region higher than 18 MeV. In the (γ, p) reaction, another strong channel is possible via $T=3/2$ states in ${}^9\text{Be}$ leaving ${}^8\text{Li}$ in $T=2$ states. However, the $T=2$ states in ${}^8\text{Li}$ are above 10.8 MeV and cannot contribute for photon

energy up to 27.7 MeV. Since proton emission analogous to the pygmy giant resonance in ${}^9\text{Be}(\gamma, n)$ is forbidden because $T=0$ states do not exist in ${}^8\text{Li}$, the extension of the pygmy giant resonance would contribute to reduce the ratio of the (γ, p) to (γ, n) cross section above 18 MeV. However, this contribution should be smaller at higher excitation energy, thus increasing the ratio, in contradiction of the experimental result.

The fine structure found in the cross sections shown in Figs. 7–10 suggests that more complex processes should be included in addition to the present simple transition. The model of free clusters should be modified to describe the real modes for ${}^9\text{Be}$, because two α cores may set into oscillation against each other and particle deexcitation from a core may be due to some complex process. An exact theoretical treatment will be necessary to explain single nucleon photoemission from ${}^9\text{Be}$.

The result of the two-cluster model calculations for this reaction via the $[{}^3\text{Li} \cdot n]$ channel in ${}^6\text{Li}$ reproduces the experimental result well [5]. In checking the present free cluster model as shown in Table V, the ${}^6\text{Li}(\gamma, n)$ reaction has significant contributions both by knockout of a neutron through the configuration of $[{}^5\text{Li} \cdot n]$ and from the elementary reaction on ${}^2\text{H}$ and ${}^4\text{He}$ via the $[\alpha \cdot d]$ configuration. The cluster configuration in ${}^7\text{Li}$ is mainly $[\alpha \cdot t]$ as shown in the table. Thus the contribution to the ${}^7\text{Li}(\gamma, n)$ reaction is only due to the elementary reaction on ${}^3\text{H}$ and ${}^4\text{He}$ (the knockout process does not appear in this case). Consequently, the cross section for ${}^7\text{Li}$ is predicted by the present model to be much smaller than that of ${}^6\text{Li}$.

In the (γ, n) reaction on ${}^6\text{Li}$ and ${}^7\text{Li}$, the states in the residual nuclei analogous to that following the (γ, p) reaction via the elementary reaction mode are at -0.33 and 3.563 MeV, respectively. Then the (γ, n) reaction resulting from the elementary reaction in ${}^6\text{Li}$ and ${}^7\text{Li}$ will appear close to the threshold and will not be separated from the predomi-

nant knockout process in ${}^6\text{Li}$. This is in contrast to the (γ, n) pygmy resonance, which is well separated from the giant dipole resonance in ${}^9\text{Be}$. The large ${}^9\text{Be}(\gamma, n)$ cross section above 18 MeV may be the result of there being two alphas in the cluster configuration of ${}^9\text{Be}$, leading to a probability for the elementary reaction on ${}^4\text{He}$ being larger than for the case of ${}^6\text{Li}$ and ${}^7\text{Li}$.

B. (γ, p_0) cross section

The (γ, p_0) reaction for ${}^9\text{Be}$ results from the elementary reaction on ${}^4\text{He}$, and it is analogous to the ${}^9\text{Be}(\gamma, n)$ reaction, leading to the lowest $T=1$ state at 16.6 MeV in ${}^8\text{Be}$ for excitations above 18 MeV in ${}^9\text{Be}$. The experimental (γ, n) reaction for ${}^9\text{Be}$ shows the $E1$ giant resonance in this energy region. The present result for the (γ, p_0) reaction includes an $E2$ contribution at the peak giant resonance as shown in Table III. This may show that some other unincluded modes may contribute to this reaction, as discussed in Sec. IV A between (γ, n) and (γ, p) cross sections.

It seems that there is a theoretical possibility for an $E2$ component by means of a proton transition from the $1p$ shell to the same shell in ${}^9\text{Be}$ through the analog states of the low-lying parent states in ${}^9\text{Li}$ [9]. Such analog states exist over several MeV in ${}^9\text{Be}$ at energies higher than 14.393 MeV. Since the shell model can approximately reproduce the photoabsorption cross section as mentioned, single-nucleon emission, such as the ${}^9\text{Be}(\gamma, n)$ and ${}^9\text{Be}(\gamma, p)$ reactions, partially indicates the shell nature as discussed for the case of the (γ, π) reaction [9].

The (γ, p_0) reaction for ${}^6\text{Li}$ can be described by the present model as involving both the knockout of a proton through $[{}^5\text{He}\cdot p]$, and the elementary reaction on ${}^2\text{H}$ and ${}^4\text{He}$ via the cluster configuration of $[\alpha\cdot d]$ as shown in Table V. The measured ${}^7\text{Li}(\gamma, p_0)$ reaction results only from the elementary reaction on ${}^3\text{H}$, which leads to a cross section that is smaller than that for ${}^6\text{Li}$.

C. (γ, d_0) cross section

This reaction on ${}^6\text{Li}$ is isospin forbidden for $E1$ absorption, and the cross section is mainly due to $E2$ absorption, resulting in a very small cross section. The cross section of this reaction has been calculated using a two-cluster model as mentioned before and agrees well with the experimental result [5]. A detailed discussion will not be made on this reaction because the $E1$ contribution is strongest in the nuclei ${}^7\text{Li}$ and ${}^8\text{Be}$, and cannot be checked by the forbidden process in ${}^6\text{Li}$.

The ${}^9\text{Be}(\gamma, d_0)$ reaction involves only the elementary reaction on ${}^4\text{He}$ as shown in Table V. Since the ${}^4\text{He}(\gamma, d)^2\text{H}$ reaction is isospin forbidden for $E1$ transitions, the cross section of ${}^9\text{Be}(\gamma, d_0)$ is expected to be too small to explain the experimental results. The cluster within a nucleus may not be exactly the same as the free particle, so that the elementary (γ, d) cross section on an α cluster may not be assumed to be as small as in ${}^4\text{He}(\gamma, d)^2\text{H}$. However, this effect cannot be expected to be so large as to explain the data. Since the angular distribution of ${}^9\text{Be}(\gamma, d_{0+1})$ shows predominantly $E1$ absorption with a slight $E2$ interference as shown in Table III, a possible contribution for ${}^9\text{Be}(\gamma, d_0)$

may be $E1$ excitation of the elementary reaction ${}^5\text{He}(\gamma, d)^3\text{H}$ via the $[{}^5\text{He}\cdot\alpha]$ component in the excited states of ${}^9\text{Be}$ [24].

The ${}^7\text{Li}(\gamma, d_0)$ cross section can be explained by the elementary reactions on ${}^3\text{H}$ and ${}^4\text{He}$ in the present model, where the ${}^3\text{H}(\gamma, d)n$ reaction is dominant for $E1$ absorption: ${}^4\text{He}(\gamma, d)^2\text{H}$ is very much suppressed as an isospin-forbidden $E2$ transition.

D. (γ, t_0) cross section

This cross section on ${}^6\text{Li}$ and ${}^7\text{Li}$ has been calculated by cluster model theories as follows. The cross section for ${}^6\text{Li}$ has been calculated by Dubovichenko and Dzhazairov-Kakhramanov through the $[{}^3\text{He}\cdot t]$ channel, and their result shows a broad resonance with a maximum cross section of about 1.5 mb in the region from 16 to 29 MeV [5]. In their paper, they made a comparison with the experimental cross section, but they did not reach any conclusion because the experimental data was poorly defined. Their result is found to possibly reproduce the recent experimental result [36], which shows a maximum cross section of about 1 mb, as shown in Fig. 15. This cross section is expected on the basis of ejection of a t through the cluster configuration $[{}^3\text{He}\cdot t]$, which is deduced to be present from polarized-photon studies of highly excited states [2]. Another contribution is expected from the elementary reaction on ${}^4\text{He}$. Early studies on the spectroscopic factor θ_0^2 of $[{}^3\text{He}\cdot t]$ in the ground state in ${}^6\text{Li}$ gave values as large as 0.68 [39], 0.45 ± 0.07 [36], and 0.8 ± 0.2 by the inverse reaction [40].

The cross section on ${}^7\text{Li}$ has also been calculated by Dubovichenko and Dzhazairov-Kakhramanov via the $[{}^4\text{He}\cdot t]$ channel in the target ground state, using the same theoretical technique as for ${}^6\text{Li}$ [5]. The result reproduces the experimental cross section, apart from structure around 11 MeV (see Fig. 15). Junghans *et al.* suggested that this structure might be correlated to a sharp rise of the (γ, n) cross section [36].

The present qualitative cluster consideration, as indicated in Table V, suggests that the (γ, t_0) reaction on ${}^6\text{Li}$ is based on two different processes; the elementary $\alpha\rightarrow p+t$ reaction in the $[\alpha\cdot d]$ ground-state configuration and ejection of a t from the $[{}^3\text{He}\cdot t]$ configuration in the excited state. Also suggested is that the ${}^7\text{Li}(\gamma, t_0)$ reaction is based on two different processes: ejection of a t from the $[{}^4\text{He}\cdot t]$ ground-state configuration and the elementary $\alpha\rightarrow p+t$ reaction in the $[\alpha\cdot t]$ configuration in the excited state. The two different transition modes in ${}^7\text{Li}$ might explain the structure around 11 MeV. The (γ, t_0) cross section of ${}^6\text{Li}$ is much larger than that of ${}^7\text{Li}$. It is therefore likely that the contribution due to ejection of a cluster t from the $[{}^3\text{He}\cdot t]$ configuration of the highly excited state in ${}^6\text{Li}$ might be the largest of all the processes mentioned above for (γ, t_0) reactions on ${}^6\text{Li}$ and ${}^7\text{Li}$.

The cross section for ${}^9\text{Be}$ is smaller than those of ${}^6\text{Li}$ and ${}^7\text{Li}$. This might suggest that the contribution to the cross section for ${}^9\text{Be}$ comes only from elementary reactions on ${}^4\text{He}$, which is a small contribution to the strong direct ejection of a t for ${}^6\text{Li}$ and ${}^7\text{Li}$.

E. $(\gamma, {}^3\text{He}_0)$ cross section

The experimental cross section for ${}^9\text{Be}$ is similar to the (γ, t_0) cross section and much smaller than that for ${}^6\text{Li}$. The only contribution to this reaction for ${}^9\text{Be}$ is ${}^4\text{He}(\gamma, {}^3\text{He})$, so that the cross section for ${}^9\text{Be}$ should be much smaller than that for ${}^6\text{Li}$, which is contributed to by direct emission of ${}^3\text{He}$.

For ${}^6\text{Li}$ the $(\gamma, {}^3\text{He}_0)$ cross section is exactly the same as for (γ, t_0) and results from ${}^3\text{He}$ ejection via the $[{}^3\text{He}\cdot t]$ configuration in the excited state in ${}^6\text{Li}$ in the present model. This is the same as t ejection leading to the ${}^6\text{Li}(\gamma, t)$ reaction. An additional elementary reaction is ${}^4\text{He}(\gamma, {}^3\text{He})n$, which is analogous to ${}^4\text{He}(\gamma, t)p$ in the case of the ${}^6\text{Li}(\gamma, t)$ reaction. The contributions of the two elementary reactions must be the same, because ${}^6\text{Li}(\gamma, t_0)$ and ${}^6\text{Li}(\gamma, {}^3\text{He}_0)$ are exactly the same. The threshold for ${}^7\text{Li}(\gamma, {}^3\text{He})$ is 31.52 MeV, so that the reaction does not appear in the present discussion.

V. SUMMARY

The cross sections for photodisintegration of ${}^9\text{Be}$ together with ${}^6\text{Li}$ and ${}^7\text{Li}$ have been discussed on the basis of the cluster model. Even under the primitive assumption of free clusters, qualitative explanations of the experimental cross sections have been achieved. The (γ, n) , (γ, d_0) , and (γ, t_0) cross sections for ${}^6\text{Li}$ and also ${}^7\text{Li}(\gamma, t_0)$ were calculated by Dubovichenko and Dzhazairov-Kakhramanov using a two-cluster model, and their results are in good agreement with experiment [4,5]. The present qualitative discussion using the simple cluster model is checked by comparison with ${}^6\text{Li}$ and ${}^7\text{Li}$ data.

Photodisintegration cross sections for ${}^9\text{Be}$ have never been calculated using a cluster model: so it is uncertain whether it applies well to ${}^9\text{Be}$. The present simple cluster model, approximated by free clusters, predicts the cross sections for ${}^9\text{Be}$ as well as those of ${}^6\text{Li}$ and ${}^7\text{Li}$. Therefore, it seems likely that if precise theoretical calculations using a many-cluster model were performed on ${}^9\text{Be}$, the photodisintegration cross sections for ${}^9\text{Be}$ would be reproduced as those for ${}^6\text{Li}$ and ${}^7\text{Li}$.

Some fine structure is seen in the experimental cross sections. This seems more pronounced for ${}^9\text{Be}$ than for ${}^6\text{Li}$ and ${}^7\text{Li}$. This may be studied by selecting an individual state represented by a cluster configuration, or shell model configuration, which may become dominant in ${}^9\text{Be}$ rather than in ${}^6\text{Li}$ and ${}^7\text{Li}$. The shell model calculations made by Ishkhanov *et al.* [22] for photoabsorption in $1p$ shell nuclei reproduces the experimental cross sections. Study of the fine structure will be an interesting problem in the future.

ACKNOWLEDGMENTS

The authors would like to thank the photoreaction group and the machine crew of the Laboratory of Nuclear Science, Tohoku University, for their help during the experiment. They are also very grateful to Dr. M. Sugawara, Dr. T. Tamae, and Dr. H. Tsubota, Tohoku University, for their help on data analysis, and to Dr. M. N. Thompson, School of Physics, the University of Melbourne, for his careful reading of the manuscript.

-
- [1] R. Ent, H. P. Block, J. F. A. van Hienen, G. van der Steenhoven, J. F. J. van den Brand, J. W. A. den Herder, E. Jans, P. H. M. Keizer, L. Lapikas, E. N. M. Quint, P. K. A. de Witt Huberts, B. L. Berman, W. J. Briscoe, C. T. Christou, D. R. Lehman, B. E. Norum, and A. Saha, *Phys. Rev. Lett.* **57**, 2367 (1986).
- [2] N. A. Burkova, V. V. Denyak, R. A. Ehramzhyan, I. G. Evseev, V. M. Khvastunov, V. P. Likhachev, S. A. Pashchuk, and M. A. Zhusupov, *Nucl. Phys.* **A586**, 293 (1995).
- [3] J. F. Dias, D. Ryckbosch, R. Van de Vyver, C. Van den Abeele, G. De Meyer, L. Van Hoorebeke, J.-O. Adler, K. I. Blomqvist, D. Nilsson, H. Ruijter, and B. Schröder, *Phys. Rev. C* **55**, 942 (1997).
- [4] S. B. Dubovichenko and A. V. Dzhazairov-Kakhramanov, *Yad. Fiz.* **58**, 635 (1995) [*Phys. At. Nucl.* **58**, 579 (1995)].
- [5] S. B. Dubovichenko and A. V. Dzhazairov-Kakhramanov, *Yad. Fiz.* **58**, 852 (1995) [*Phys. At. Nucl.* **58**, 788 (1995)]. The vertical unit of Fig. 7 in this reference should be mb not μb .
- [6] N. Burtebaev, A. D. Duisebaev, G. N. Ivanov, and S. B. Sakuta, *Yad. Fiz.* **58**, 596 (1995) [*Phys. At. Nucl.* **58**, 540 (1995)].
- [7] A. Okihana, K. Ushiro, T. Yoshimura, S. Kakigi, and T. Sekioka, *Nucl. Phys.* **A614**, 71 (1997).
- [8] V. I. Kukulin, V. N. Pomerantsev, Kh. D. Razikov, V. T. Voronchev, and G. G. Ryzhikh, *Nucl. Phys.* **A586**, 151 (1995).
- [9] K. Shoda, S. Tôyama, K. Takeshita, T. Kobayashi, and H. Tsubota, *Phys. Rev. C* (submitted).
- [10] J. Ahrens, H. Borchert, K. H. Czock, H. B. Eppler, H. Gimm, H. Gundrum, M. Kröning, P. Riehn, G. Sita Ram, A. Zieger, and B. Ziegler, *Nucl. Phys.* **A251**, 479 (1975).
- [11] C. Becchi, L. Meneghetti, M. Sanzone, and S. Vitale, *Nucl. Phys.* **59**, 375 (1964).
- [12] F. M. Clikeman, A. J. Bureau, and M. G. Stewart, *Phys. Rev.* **126**, 1822 (1962).
- [13] U. Kneissl, G. Kuhl, K. H. Leister, and A. Weller, *Nucl. Phys.* **A247**, 91 (1975).
- [14] V. P. Chizhov, A. P. Komar, L. A. Kul'chitsky, A. V. Kulikov, E. D. Makhnovsky, and Yu. M. Volkov, *Nucl. Phys.* **34**, 562 (1962).
- [15] B. Čujec, *Nucl. Phys.* **37**, 396 (1962).
- [16] V. P. Denisov and L. A. Kul'chitskii, *Yad. Fiz.* **3**, 268 (1966); *Sov. J. Nucl. Phys.* **3**, 192 (1966).
- [17] S. Costa, L. Pasqualini, G. Piragino, and L. Roasio, *Nuovo Cimento B* **42**, 306 (1966).
- [18] K. Shoda, M. Sugawara, T. Saito, and H. Miyase, *Nucl. Phys.* **A221**, 125 (1974).
- [19] W. C. Barber and T. Wiedling, *Nucl. Phys.* **18**, 575 (1960).
- [20] I. C. Nascimento, E. Wolyneć, and D. S. Onley, *Nucl. Phys.* **A246**, 210 (1975).
- [21] R. N. H. Haslam, L. Katz, E. H. Crosby, R. G. Summers-Gill,

- and A. G. W. Cameron, *Can. J. Phys.* **31**, 210 (1952).
- [22] B. S. Ishkhanov, I. M. Kapitonov, V. G. Neudachin, and R. A. Éramzhyan, *Fiz. Elem. Chastits At. Yadra* **12**, 905 (1981) [*Sov. J. Part. Nucl.* **12**, 362 (1981)].
- [23] G. Feldman, M. J. Balbes, L. H. Kramer, J. Z. Williams, H. R. Weller, and D. R. Tilley, *Phys. Rev. C* **42**, R1167 (1990).
- [24] K. Langanke, in *Advances in Nuclear Physics*, edited by J. W. Negele and E. Vogt (Plenum Press, New York, 1994), Vol. 21, p. 85.
- [25] D. Baye and P. Descouvemont, *J. Phys. Soc. Jpn.* **58**, 103 (1989).
- [26] L. Majling, V. I. Kukulin, and Yu. F. Smirnov, *Phys. Lett.* **27B**, 487 (1968); *Czech. J. Phys., Sect. B* **18**, 1561 (1968); R. Shackleton, Ph.D. thesis, University of Melbourne, 1971.
- [27] A. Csóto and G. M. Hale, *Phys. Rev. C* **55**, 2366 (1997).
- [28] M. Sanzone, in *International School of Intermediate Energy Nuclear Physics*, edited by R. Bergere, S. Costa, and C. Schaerf (World Scientific, Singapore, 1986), p. 78.
- [29] D. D. Faul, B. L. Berman, P. Meyer, and D. L. Olson, *Phys. Rev. C* **24**, 849 (1981).
- [30] D. M. Skopik, D. H. Beck, J. Asai, and J. J. Murphy II, *Phys. Rev. C* **24**, 1791 (1981).
- [31] B. L. Berman, D. D. Faul, P. Meyer, and D. L. Olson, *Phys. Rev. C* **22**, 2273 (1980).
- [32] G. Ticcioni, S. N. Gardiner, J. L. Matthews, and R. O. Owens, *Phys. Lett.* **46B**, 369 (1973).
- [33] H. G. Clerc, R. J. Stewart, and R. C. Morrison, *Phys. Lett.* **18**, 316 (1965).
- [34] Yu. M. Arkatov, P. I. Vatset, V. I. Voloshchuk, I. M. Prokhorets, A. F. Khodyachikh, and V. I. Chmil', *Yad. Fiz.* **16**, 12 (1972) [*Sov. J. Nucl. Phys.* **16**, 6 (1973)].
- [35] B. L. Berman and S. C. Fultz, *Rev. Mod. Phys.* **47**, 713 (1975).
- [36] G. Junghans, K. Bangert, U. E. P. Berg, R. Stock, and K. Wienhard, *Z. Phys. A* **291**, 353 (1979).
- [37] D. M. Skopik, E. L. Tomusiak, E. T. Dressler, Y. M. Shin, and J. J. Murphy II, *Phys. Rev. C* **14**, 789 (1976); H. Taneichi, H. Ueno, K. Shoda, Y. Kawazoe, and T. Tsukamoto, *Nucl. Phys.* **A448**, 315 (1986); R. G. H. Robertson, P. Dyer, R. A. Werner, R. C. Melin, T. J. Bowles, A. B. McDonald, C. C. Ball, W. G. Davis, and F. D. Earle, *Phys. Rev. Lett.* **47**, 1867 (1981).
- [38] A. Buchnea, R. G. Johnson, and K. G. McNeill, *Can. J. Phys.* **56**, 47 (1978).
- [39] Y. M. Shin, D. M. Skopik, and J. J. Murphy, *Phys. Lett.* **55B**, 297 (1975).
- [40] E. Ventura, J. R. Calarco, W. E. Meyerhof, and A. M. Young, *Phys. Lett.* **46B**, 364 (1973).